Received: 25 January 2023 | Revised: 11 April 2023 | Accepted: 17 April 2023

DOI: 10.1002/jimd.12619

ORIGINAL ARTICLE

JIMD SSIEM WILEY

A mouse mutant deficient in both neuronal ceroid lipofuscinosis-associated proteins CLN3 and TPP1

David E. Sleat[1,2] | Whitney Banach-Petrosky[1] | Katherine E. Larrimore[1] | Yuliya Nemtsova[1] | Jennifer A. Wiseman[1] | Allison Najafi[3] | Dymonn Johnson[4] | Timothy A. Poole[4] | Keigo Takahashi[4] | Jonathan D. Cooper[3,4,5,6] | Peter Lobel[1,2]

[1]Center for Advanced Biotechnology and Medicine, Rutgers University, Piscataway, New Jersey, USA

[2]Department of Biochemistry and Molecular Biology, Robert Wood Johnson Medical School, Rutgers Biomedical Health Sciences, Rutgers University, Piscataway, New Jersey, USA

[3]The Lundquist Institute (formerly Los Angeles Biomedical Research Institute), Harbor-UCLA Medical Center, and David Geffen School of Medicine, University of California, Torrance, California, USA

[4]Department of Pediatrics, Division of Genetics and Genomic Medicine, Washington University in St Louis, School of Medicine, St Louis, Missouri, USA

[5]Department of Genetics, Division of Genetics and Genomic Medicine, Washington University in St Louis, School of Medicine, St Louis, Missouri, USA

[6]Department of Neurology, Division of Genetics and Genomic Medicine, Washington University in St Louis, School of Medicine, St Louis, Missouri, USA

Correspondence
David E. Sleat and Peter Lobel, Center for Advanced Biotechnology and Medicine, Rutgers University, Piscataway, NJ, USA.
Email: sleat@cabm.rutgers.edu and lobel@cabm.rutgers.edu

Funding information
Batten Disease Support and Research Association; Beyond Batten Disease Foundation; Hope4Bridget; NINDS, Grant/Award Numbers: R21NS088786, R01NS37918

Communicating Editor: Roberto Giugliani

Abstract

Late-infantile neuronal ceroid lipofuscinosis (LINCL) and juvenile neuronal ceroid lipofuscinosis (JNCL) are inherited neurodegenerative diseases caused by mutations in the genes encoding lysosomal proteins tripeptidyl peptidase 1 (TPP1) and CLN3 protein, respectively. TPP1 is well-understood and, aided by animal models that accurately recapitulate the human disease, enzyme replacement therapy has been approved and other promising therapies are emerging. In contrast, there are no effective treatments for JNCL, partly because the function of the CLN3 protein remains unknown but also because animal models have attenuated disease and lack robust survival phenotypes. Mouse models for LINCL and JNCL, with mutations in *Tpp1* and *Cln3*, respectively, have been thoroughly characterized but the phenotype of a double *Cln3*/*Tpp1* mutant remains unknown. We created this double mutant and find that its phenotype is essentially indistinguishable from the single $Tpp1^{-/-}$ mutant in terms of survival and brain pathology. Analysis of brain proteomic changes in the single $Tpp1^{-/-}$ and double $Cln3^{-/-}$;$Tpp1^{-/-}$ mutants indicates largely overlapping sets of altered proteins and reinforces earlier studies that highlight GPNMB, LYZ2, and SERPINA3 as promising biomarker candidates

in LINCL while several lysosomal proteins including SMPD1 and NPC1 appear to be altered in the *Cln3*$^{-/-}$ animals. An unexpected finding was that *Tpp1* heterozygosity significantly decreased lifespan of the *Cln3*$^{-/-}$ mouse. The truncated survival of this mouse model makes it potentially useful in developing therapies for JNCL using survival as an endpoint. In addition, this model may also provide insights into CLN3 protein function and its potential functional interactions with TPP1.

KEYWORDS

CLN3 protein, mouse, neuronal ceroid lipofuscinosis, tripeptidyl peptidase 1

1 | INTRODUCTION

The neuronal ceroid lipofuscinoses (NCLs) are a group of more than a dozen genetically distinct but similar lysosomal storage diseases.[1] Characterized by an accumulation of autofluorescent storage material within the lysosome, NCLs are neurodegenerative and progressive diseases that are manifested by seizures, loss of vision, and eventual loss of mental capacity. Onset is typically in childhood and these diseases result in premature death. Two of the most frequently encountered NCL diseases are the classical late-infantile and juvenile forms (LINCL and JNCL, respectively). LINCL results from mutations in the gene encoding tripeptidyl peptidase 1 (TPP1, formerly designated CLN2),[2,3] a soluble lysosomal serine protease.[4–6] Disease in LINCL typically presents at around 4 years of age and lifespan is ~8–15 years.[1] JNCL is caused by mutations in a gene encoding a lysosomal transmembrane protein, CLN3.[7] JNCL has a later onset and is more slowly progressing than LINCL, with first signs of disease (typically problems with vision) at around 8 years and patients frequently surviving into the second or third decade of life.[1] Despite differences in disease timeline and genetic etiology, LINCL and JNCL have a number of similarities including lysosomal storage of subunit c of mitochondrial ATP synthase (SCMAS).[8]

There is considerable focus on the development of effective therapies for NCL diseases and LINCL is leading the way. Enzyme replacement therapy has been clinically approved for LINCL[9,10] and there is interest in gene therapy, with promising results obtained in animal models,[11–15] and clinical studies have been conducted.[16,17] Both enzyme replacement therapy (ERT) and gene-therapy rely upon the fact that TPP1 is a soluble lysosomal protein.[2] In ERT, exogenously-administered recombinant protein can be taken up by numerous cells by endocytosis and delivered to the lysosome, while in gene therapy, a only a proportion of cells are transduced but these can overproduce and secrete enzyme that is taken up by untransduced cells. In addition, there are LINCL animal models[18,19] with well-defined phenotypes that accurately recapitulate the human disease and these have been integral in testing treatment strategies.

There is currently no approved therapy for JNCL and this reflects several major obstacles. First, CLN3 is a transmembrane protein,[7] which excludes replacement treatment using exogenously administered recombinant protein. There is interest in gene therapy for JNCL[20] but because CLN3 is an integral membrane protein, non-transduced cells will not express the missing protein. Thus, if the underlying metabolic defect is cell autonomous, cross-protection between transduced and untransduced cells may not be possible, and a very high proportion of cells will require transduction for effective therapy. Second, there is a fundamental lack of understanding of the cellular function of the CLN3 protein. It has been implicated in numerous cellular activities including lysosomal pH homeostasis, endocytosis, autophagy, apoptosis, lysosomal enzyme transport, and others.[21] While the precise function of CLN3 is yet to be definitively established, a recent study has established that glycerophosphodiesters accumulate within the lysosome in the absence of CLN3,[22] raising the possibility the CLN3 is a lysosomal transporter for these lipids. Regardless, mechanism-based approaches to treatment for JNCL are currently not an option. Third, animal models for JNCL do not present a robust phenotype, especially with respect to survival. There are several mouse models for JNCL[23–26] and their phenotypes are very similar but in all, disease is highly attenuated compared to mouse models of other NCL diseases.

In this study, we have created mice that are defective in both CLN3 protein and TPP1 with the rationale that the phenotype of a double mutant may provide insights into CLN3 protein function and possible functional interactions with TPP1. In terms of survival, pathology, and proteomic changes within the brain, the phenotype of the double mutant is essentially indistinguishable from mice

that lack TPP1 alone. However, we find that the lifespan of the *Cln3*$^{-/-}$ mouse model is shortened in a *Tpp1* heterozygous background. While the physiological implications of this are unclear, this does potentially provide a mouse model with a clear JNCL survival phenotype that may be of value in therapeutic testing.

2 | METHODS

2.1 | Animals

Mice were maintained and used following protocols approved by the Rutgers University and Robert Wood Johnson Medical School Institutional Animal Care and Use Committee ("Preclinical evaluation of therapy in an animal model for LINCL," protocol I09-0274-4). *Tpp1*$^{-/-}$ mice[19] were either in an *Nnt*$^{-/-}$[27] C57BL/6J or *Nnt*$^{+/+}$ C57BL/6 strain background. *Cln3*$^{-/-}$ mice[28] were in a C57BL/6J genetic background. Animals arising from crosses between C57BL/6 *Tpp1*$^{-/-}$ mice and C57BL/6J *Cln3*$^{-/-}$ mice are in a mixed C57BL6 substrain background designated here as C57BL/6×6J and they are a mixture of *Nnt*$^{+/+}$, *Nnt*$^{+/-}$ and *Nnt*$^{-/-}$ genotypes. Genotyping of *Tpp1*$^{-/-}$ and *Cln3*$^{-/-}$ mice was conducted as described.[19,28] Experimental cohorts contained ~equal numbers of males and female animals and were analyzed at ~120 days of age. For biochemical analyses, animals were deeply anesthetized with sodium pentobarbital/phenytoin (a 1:4 dilution of Euthasol; Delmarva Laboratories, Midlothian, VA) and euthanized by transcardial perfusion with 0.9% saline. Brains were dissected and frozen on dry ice. For histopathology, mice were anesthetized, perfused with saline then perfusion-fixed with 4% paraformaldehyde in PBS. Brains were excised, fixed for 48 h in 4% paraformaldehyde in PBS, and then transferred to 30% sucrose/PBS at 4°C until they sunk.

2.2 | Quantitative mass spectrometry

Sample preparation and quantitative mass spectrometry on whole brain extracts were conducted as described previously[29] and parameters for mass spectrometry, peak list generation, and database searching are summarized in Table S1. In brief, detergent-solubilized extracts were prepared, proteins were digested in-solution sequentially with trypsin (specificity, carboxyl side of K and R) and endoprotease LysC (specificity, carboxyl side of K) and the resulting peptides labeled with TMT11-plex isobaric reagents (ThermoFisher Scientific). Labeled samples were pooled and analyzed by synchronous precursor selection MS3 on a Lumos Tribrid instrument (ThermoFisher Scientific).

2.3 | Database searching

Peak lists were generated using Proteome Discoverer 2.2 (ThermoFisher Scientific) and data were searched using a local implementation of the Global Proteome Machine (GPM)[30,31] using search parameters shown in Table S1. Protein assignments are shown in Table S2. Mass spectrometry files (mgf and raw files, GPM search files, and Excel files denoting protein assignments, peptide-spectrum matches, and corresponding reporter ion intensities) are archived in the MassIVE (http://massive.ucsd.edu) and ProteomeXchange (http://www.proteomexchange.org/) repositories in submission MSV000087613.

2.4 | Normalization and statistical analyses of mass spectrometry data

TMT-11 reporter ion intensities were normalized and analyzed as described previously.[32] In brief, reporter ion intensity data were extracted from peak list files using custom in-house scripts (https://github.com/cgermain/IDEAA), then spectra were normalized to total reporter ion intensity per channel to correct for differences in labeling efficiency and/or amounts of protein labeled. Spectral assignments with reporter ion intensities are shown in Table S2. Peptides were first filtered for fully tryptic cleavage, no missed cleavage sites, and complete iTRAQ labeling of lysines and amino termini. Peptides were then filtered to remove those containing posttranslational modifications that may increase variability in the data (i.e., asparagine or glutamine deamidation, methionine dioxidation, tryptophan mono- and dioxidation, and isobaric labeling of tyrosine at positions other than the amino terminus). For selected comparisons, ratios of expression and q-values corrected for multiple comparisons using the Benjamini–Hochberg procedure[33] were generated using a nested procedure that accounts for variability at both peptide and protein level[32] (Table S3).

2.5 | Immunostaining

For immunohistochemistry, a one in six series of coronal brain sections from each mouse were stained using a modified immunofluorescence protocol[34] for the astrocyte marker glial fibrillary associated protein (GFAP, rabbit anti-GFAP, 1:1000, DAKO), and the microglial marker CD68 (rat anti-mouse CD68, 1:400, Bio-Rad). Briefly, 40 μm coronal sections were mounted on Superfrost Plus slides (Fisher Scientific) and air-dried for 30 min, slides were then blocked in a 15% serum solution in 2% TBS-T (1× Tris Buffered Saline, pH 7.6 with 2% Triton-X100, Fisher Scientific) for 1 h. Slides were then incubated in primary antibody in 10%

serum solution in 2% TBS-T for 2 h, washed three times in 1xTBS, and incubated with fluorescent Alexa-Fluor labeled IgG secondary antibodies (Alexa-Fluor goat anti-rabbit 488, goat anti-rat 546, Invitrogen) in 10% serum solution in 2% TBS-T for 2 h. Slides were washed three times in 1xTBS and incubated in a 1× solution of TrueBlack lipofuscin autofluoresence quencher (Biotium, Fremont, CA) in 70% ethanol for 2 min before rinsing with 1xTBS. Slides were cover-slipped in Fluoromount-G mounting medium with DAPI (Southern Biotech, Birmingham, AL).

2.6 | Thresholding image analysis

To analyze the degree of glial activation in the gray matter (GFAP positive astrocytes + CD68 positive microglia) a semiautomated thresholding image analysis method was used with *Image-Pro Premier software* (Media Cybernetics). Briefly, stained sections were scanned using a Zeiss AxioScan Z1 slide scanner at the Washington University Center for Cellular Imaging (WUCCI), at 10× magnification of each one in six series of sections per animal followed by demarcation of all regions of interest. Images were subsequently analyzed using *Image-Pro Premier* (Media Cybernetics) using an appropriate threshold that selected the foreground immunoreactivity above the background. This threshold was then applied as a constant to all subsequent images analyzed per batch of animals and reagent used to determine the specific area of immunoreactivity for each antigen. Measurements for histological processing were performed blind to genotype and statistical analyses were performed using GraphPad Prism version 8.0.0 for MacOS. Data were analyzed using two-way ANOVA with a post hoc Bonferroni correction, with a $p \leq 0.05$ considered significant.

2.7 | Survival statistics

Survival curves were compared using log-rank tests in GraphPad Prism 9.1 (GraphPad Software, San Diego, CA, www.graphpad.com).

2.8 | TPP1 enzyme assay

TPP1 was measured using an endpoint assay with Ala-Ala-Phe-AMC substrate as described previously.[5] For TPP1 assay in the presence of glycerophosphodiesters, TPP1 activity was again measured by endpoint assay with 200 μM Ala-Ala-Phe-AMC and 1 or 10 mM L-α-Glycerophosphorylcholine (Sigma) or 100 μM Glycerophosphoinositol (Echelon), each dissolved in water.

3 | RESULTS

3.1 | Breeding strategy

Our original plan for generating all required genotypes as littermates was to conduct dihybrid crosses using animals that were heterozygous for both *Tpp1* and *Cln3* mutations. Analysis of transmission ratios indicated that offspring were not generated in the predicted ratios (data not shown) with lower than predicted numbers of both $Tpp1^{-/-};Cln3^{-/-}$ and $Tpp1^{+/+};Cln3^{+/+}$ animals. This reflects gene linkage with both *Tpp1* and *Cln3* located on chromosome 7 in the mouse (*Tpp1* location: Chr 7 E3; 7 55.97 cM, *Cln3* location: Chr 7 F3; 7 69.16 cM). Subsequently, double knockout animals were generated by $Tpp1^{-/-};Cln3^{-/-}$ x $Tpp1^{-/-};Cln3^{-/-}$ or $Tpp1^{-/-};Cln3^{-/+}$ x $Tpp1^{+/-};Cln3^{-/-}$ matings.

3.2 | Survival

Survival curves and statistical comparisons are shown in Figure 1, and Table 1. Given the substantial differences in survival, animals on a $Tpp1^{-/-}$ background are shown in Figure 1A and animals on a $Tpp1^{+/-}$ or $Tpp1^{+/+}$ background are shown in Figure 1B,C.

$Tpp1^{-/-};Cln3^{-/-}$, $Tpp1^{-/-};Cln3^{+-}$ and $Tpp1^{-/-};Cln3^{+/+}$ animals in the mixed C57BL/6×6J background had median survivals between 120 and 124 days (Table 1). Survival of $Tpp1^{-/-};Cln3^{-/-}$ (median 124 days) was slightly but significantly ($p = 0.0114$) shorter than $Tpp1^{-/-};Cln3^{+/+}$ littermates (median 120 days) and the survival curve of $Tpp1^{-/-};Cln3^{-/-}$ mice was somewhat rectangularized compared to the $Tpp1^{-/-};Cln3^{+/+}$ mice (Figure 1A). This may be an effect of the *Cln3* mutation on the $Tpp1^{-/-}$ phenotype but most likely reflects a subtle difference in the genetic background of the animals. The *Tpp1* mutant allele used for these studies was backcrossed against C57BL/6[19] as was the *Cln3* allele.[37] However, the substrain background of the two mutants differ in that the $Tpp1^{-/-}$ mice were $Nnt^{+/+}$ while the $Cln3^{-/-}$ mice were $Nnt^{-/-}$.[29] Mutations in *Nnt* vary in different C57BL/6 substrains[27] and the $Nnt^{-/-}$ genotype arose at Jackson Laboratories and is designated as C57BL/6J. Subtle differences in survival likely reflect differences in substrain given that isogenic $Tpp1^{-/-}$ mice in an $Nnt^{-/-}$ C57BL/6J background have a significantly ($p < 0.0001$) shorter lifespan (median 112 days) as the same mutant in the isogenic $Nnt^{+/+}$ C57BL/6 background (median 137 days). Regardless, the primary conclusion is that there was no marked difference in survival phenotype of the $Tpp1^{-/-}Cln3^{-/-}$ double mutant and $Tpp1^{-/-}Cln3^{+/+}$ single mutant animals.

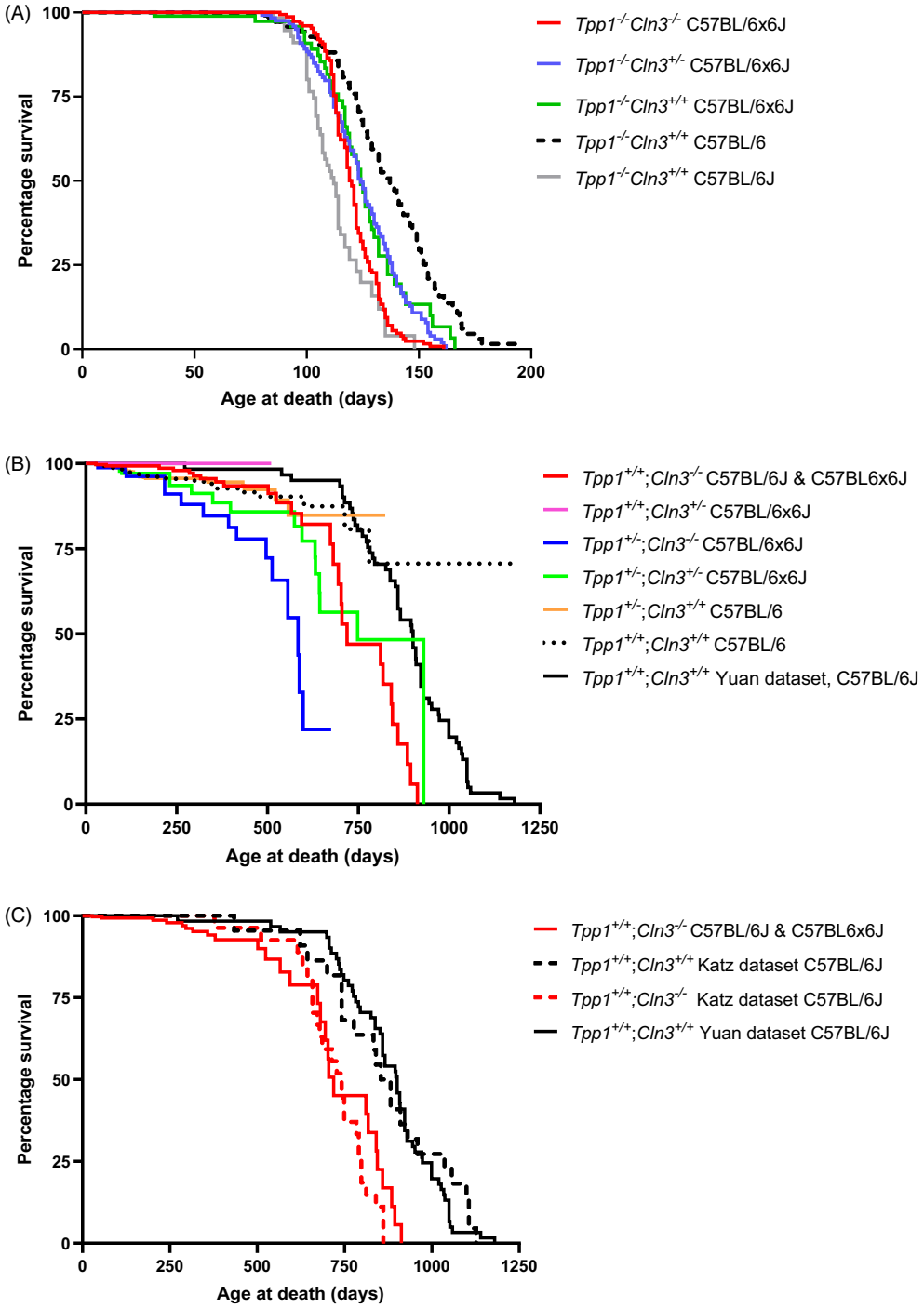

FIGURE 1 Survival analysis of Tpp1 and Cln3 mice.
(A) Survival analysis of mice in a $Tpp1^{-/-}$. Data are included for $Tpp1^{-/-}$;$Cln3^{+/+}$ in a C57BL/6 $Nnt^{+/+}$ background, a C57BL/6J $Nnt^{-/-}$ background and a mixed C57BL6 and C57BL6/J background (C57BL/6×6J).
(B) Survival analysis of mice in a $Tpp1^{+/-}$ or $Tpp1^{+/+}$ background. The Yuan survival dataset[35] was obtained from Jackson Laboratories (https://phenome.jax.org/projects/Yuan2) and comprised male and female mice in a C57BL/6J substrain background.
(C) Comparison of survival of $Tpp1^{+/+}$;$Cln3^{-/-}$ animals from the current study with historical data for wild-type and $Tpp1^{+/+}$;$Cln3^{-/-}$ animals.[36] Data were obtained from ~equal numbers of male and female animals. Median survival and number of animals analyzed per genotype are shown in Table 1.

Survival of mutant animals in $Tpp1^{+/-}$ or $Tpp1^{+/+}$ backgrounds are shown in Figures 1B,C. Note that we collected limited survival data for wild-type animals and therefore include data from C57BL/6J animals from another study ("Yuan dataset").[35] Survival of *Tpp1* heterozygotes did not differ significantly ($p = 0.1635$) from the Yuan dataset of wild-type animals (median survival 901 days) (Figure 1B). We did not collect survival data for $Tpp1^{+/+}$;$Cln3^{+/-}$ animals but given that heterozygosity for *Tpp1* did not affect survival, we predict no significant differences in survival of *Cln3* heterozygotes when compared to wild-type. Survival of $Tpp1^{+/-}$;$Cln3^{+/-}$ double heterozygote mice (median 748 days) was similar to the single $Cln3^{-/-}$ mice (p = 0.5719) and was also significantly shorter than wild-type animals ($p = 0.0014$). *Tpp1* heterozygosity resulted in decreased survival of $CLN3^{-/-}$ animals (median 584 days) which was significantly ($p < 0.0001$) shorter than that of the $Tpp1^{+/+}$;$Cln3^{-/-}$ animals. Overall, these data indicate that heterozygosity for *Tpp1* resulted in decreased survival of both $Cln3^{+/-}$ and $Cln3^{-/-}$ animals.

TABLE 1 Survival statistics for $Tpp1^{-/-}$ animals.

Genotype	Total n /number of events	Median survival	Log-rank (Mantel–Cox) test		Significant
			p value	Compared to	
$Tpp1^{-/-}$;$Cln3^{-/-}$(C57BL/6×6J)	204/134	120	0.0114 0.0017	$Tpp1^{-/-}$;$Cln3^{+/+}$ (C57BL6×6J) $Tpp1^{-/-}$;$Cln3^{+/-}$ (C57BL6×6J)	No Yes
$Tpp1^{-/-}$;$Cln3^{+/-}$(C57BL/6×6J)	126/108	124	0.5239	$Tpp1^{-/-}$;$Cln3^{+/+}$ (C57BL6×6J)	No
$Tpp1^{-/-}$;$Cln3^{+/+}$ (C57BL/6×6J)	52/45	124	0.0007	$Tpp1^{-/-}$;$Cln3^{+/+}$ (C57BL6)	Yes
*$Tpp1^{-/}$;$Cln3^{+/+}$ (C57BL/6)	149/105	137	<0.0001	$Tpp1^{-/-}$;$Cln3^{+/+}$ (C57BL6J)	Yes
*$Tpp1^{-/}$;$Cln3^{+/+}$ (C57BL/6J)	22/47	112			
*$Tpp1^{+/+}$;$Cln3^{+/+}$ (C56BL/6)	1144/44	Not defined	0.4072	$Tpp1^{+/+}$;$Cln3^{+/+}$ (Yuan dataset, C57BL/6J)	No
$Tpp1^{+/+}$;$Cln3^{+/+}$ (Yuan dataset)	61/61	901			
$Tpp1^{+/-}$;$Cln3^{-/-}$(C57BL/6×6J)	68/15	584	<0.0001	$Tpp1^{+/+}$;$Cln3^{-/-}$ (C57BL/6J and C57BL/6×6J)	Yes
$Tpp1^{+/-}$;$Cln3^{+/-}$(C57BL/6×6J)	228/18	748	0.5719 0.0014	$Tpp1^{+/+}$;$Cln3^{-/-}$ $Tpp1^{+/+}$;$Cln3^{+/+}$ (Yuan dataset)	No Yes
*$Tpp1^{+/-}$;$Cln3^{+/+}$ (C57BL6)	1442/49	Undefined	0.1635	$Tpp1^{+/+}$;$Cln3^{+/+}$ (Yuan dataset)	No
*$Tpp1^{+/+}$;$Cln3^{-/-}$(C57BL/6J and C57BL/6×6J)	289/27	719	<0.0001	$Tpp1^{+/+}$;$Cln3^{+/+}$ (Yuan dataset)	Yes
$Tpp1^{+/+}$;$Cln3^{-/-}$ (Katz dataset, C57BL/6J)	27/27	742	0.2339	$Tpp1^{+/+}$;$Cln3^{-/-}$ (C57BL/6J and C57BL/6×6J)	No

Note: Survival data were obtained from littermates from crosses between double *Tpp1* and *Cln3* mutant crosses unless indicated otherwise (* for single mutant crosses). Significance for the Log-rank tests conducted below was evaluated after correction of *p* values for multiple comparisons using the Bonferroni method.

Survival of our $Tpp1^{+/+}$; $Cln3^{-/-}$ mice (median 719 days) was not significantly different ($p = 0.2339$) from historical data from a different but similar JNCL knockout mouse model (742 days)[36] (Figure 1C). However, the survival of both *Cln3* mutants was significantly reduced compared to wild-type mice ($p < 0.0001$).

3.3 | Pathology

In order to compare brain pathology in the double mutant $Tpp1^{-/-}Cln3^{-/-}$ and single mutant $Tpp1^{-/-}$ animals, animals were euthanized at their median lifespan of ~120 days. Sections were analyzed by immunofluorescence for the simultaneous detection of markers of glial activation, (CD68 in microglia and GFAP in astrocytes) in two brain regions where pronounced glial activation is consistently observed in multiple NCL mouse models: the barrel field of the somatosensory cortex (S1BF) and the region encompassing the medial and lateral ventral posterior nuclei of the thalamus (VPM/VPL). As expected, immunostaining for either GFAP or CD68 was present at very low levels in animals with a $Tpp1^{+/-}$ or $Tpp1^{+/+}$ genotype irrespective of *Cln3* genotype. In these animals, only very faintly stained GFAP-positive astrocytes or CD68-positive microglia (Figure 2) were present. Consistent with previous observations,[38] marked activation of both astrocytes and microglia was detected in the S1BF and VPM/VPL of $Tpp1^{-/-}Cln3^{+/+}$ animals, with pronounced upregulation of these markers and corresponding changes in cellular morphology. Similar levels of pronounced glial activation were detected in the S1BF and VPM/VPL of double mutant $Tpp1^{-/-}Cln3^{-/-}$ animals, with similar degrees of cellular hypertrophy of both astrocytes and microglia apparent to those seen in $Tpp1^{-/-}Cln3^{+/+}$ animals. Thresholding image analysis confirmed these qualitative observations with significant elevation of both GFAP and CD68 immunoreactivity in both brain regions of $Tpp1^{-/-}Cln3^{+/+}$ and $Tpp1^{-/-}Cln3^{-/-}$ animals compared to other genotypes (Figure 3). Although the individual levels of GFAP and CD68 immunoreactivity differed to some extent between $Tpp1^{-/-}Cln3^{+/+}$ and $Tpp1^{-/-}Cln3^{-/-}$ animals, there were no significant differences for either antigen in either

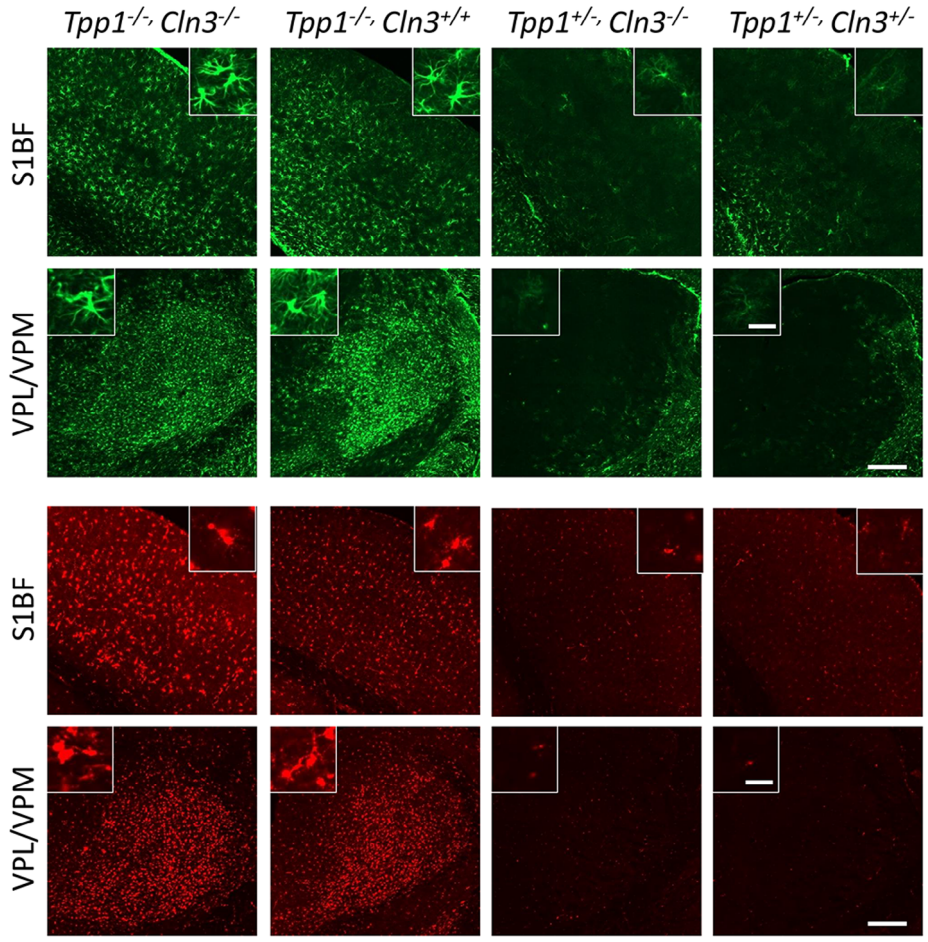

FIGURE 2 Astrocytosis and microglial activation in 120-day old $Tpp1^{-/-}Cln3^{+/+}$ and $Tpp1^{-/-}Cln3^{-/-}$ animals. Immunofluorescence staining for the astrocyte marker glial fibrillary associated protein (GFAP, green) and microglial marker CD68 (red) reveals profound astrocytosis and microglial activation respectively, in the primary somatosensory cortex (S1BF) and ventral posterior thalamic nuclei (VPM/VPL) of both $Tpp1^{-/-}Cln3^{+/+}$ and $Tpp1^{-/-}Cln3^{-/-}$ animals, compared to relatively low levels of GFAP and CD68 immunoreactivity in the gray matter of $Tpp1^{+/-}Cln3^{-/-}$ and $Tpp1^{+/-}Cln3^{+/-}$, which is comparable to previously published data from wild-type mice. Scale bar = 100 and 25 μm in inserts.

brain region between animals of these genotypes. This broad similarity between $Tpp1^{-/-}Cln3^{+/+}$ and $Tpp1^{-/-}Cln3^{-/-}$ animals in terms of the extent of glial activation is consistent with the similarities observed in the survival phenotypes of these mutants. While we did not measure autofluorescence, lysosomal storage, and neuronal loss, we would predict these to be similar or identical in the $Tpp1^{-/-}Cln3^{+/+}$ and $Tpp1^{-/-}Cln3^{-/-}$ animals given the similarities in glial activation pathology and survival phenotypes. Overall, *Cln3* genotype had no observable effect on the pathology of $Tpp1^{-/-}$ animals at the age tested (~100 days). This provides further evidence that *Cln3* defects do not exacerbate the LINCL phenotype in these animals.

3.4 | Proteomic analysis

We conducted a proteomic analysis on brain samples from the Tpp1 and Cln3 mutant mice with the goal of identifying changes that might correlate with disease survival and may shed light on the respective cellular functions of these proteins. In addition, given that earlier proteomic studies failed to identify any informative brain expression changes in $Cln3^{-/-}$ mice,[29] we hypothesized that changes related to *Cln3* mutation could be exacerbated and thus possibly easier to detect in a Tpp1 mutant background. Proteins in brain extracts from animals at ~105 days were identified and quantified using isobaric labeling mass spectrometry. In Figure 4, we compared various genotypes of interest using volcano plots, a scatter plot that allows comparison of effect size with the probability of significant difference. Q values (i.e., *p* values adjusted for multiple comparisons found using the Benjamini–Hochberg false discovery rate method) were calculated by comparing reporter ion intensities for all individual spectra assigned to a given protein from all biological replicates for each genotype.

A number of significant changes in protein expression were detected when $Tpp1^{-/-}$ animals were compared with wild-type including elevation of GPNMB, LYZ2, SERPINA3N, and various lysosomal proteins including several cathepsins (Table S4). When double mutant $Tpp1^{-/-}$;$Cln3^{-/-}$ animals were compared to wild-type, we identified very similar changes in protein expression for the most part as illustrated by the high degree of correlation between fold changes in expression compared to wild-type in $Tpp1^{-/-}$;$Cln3^{+/+}$ and $Tpp1^{-/-}$;$Cln3^{-/-}$

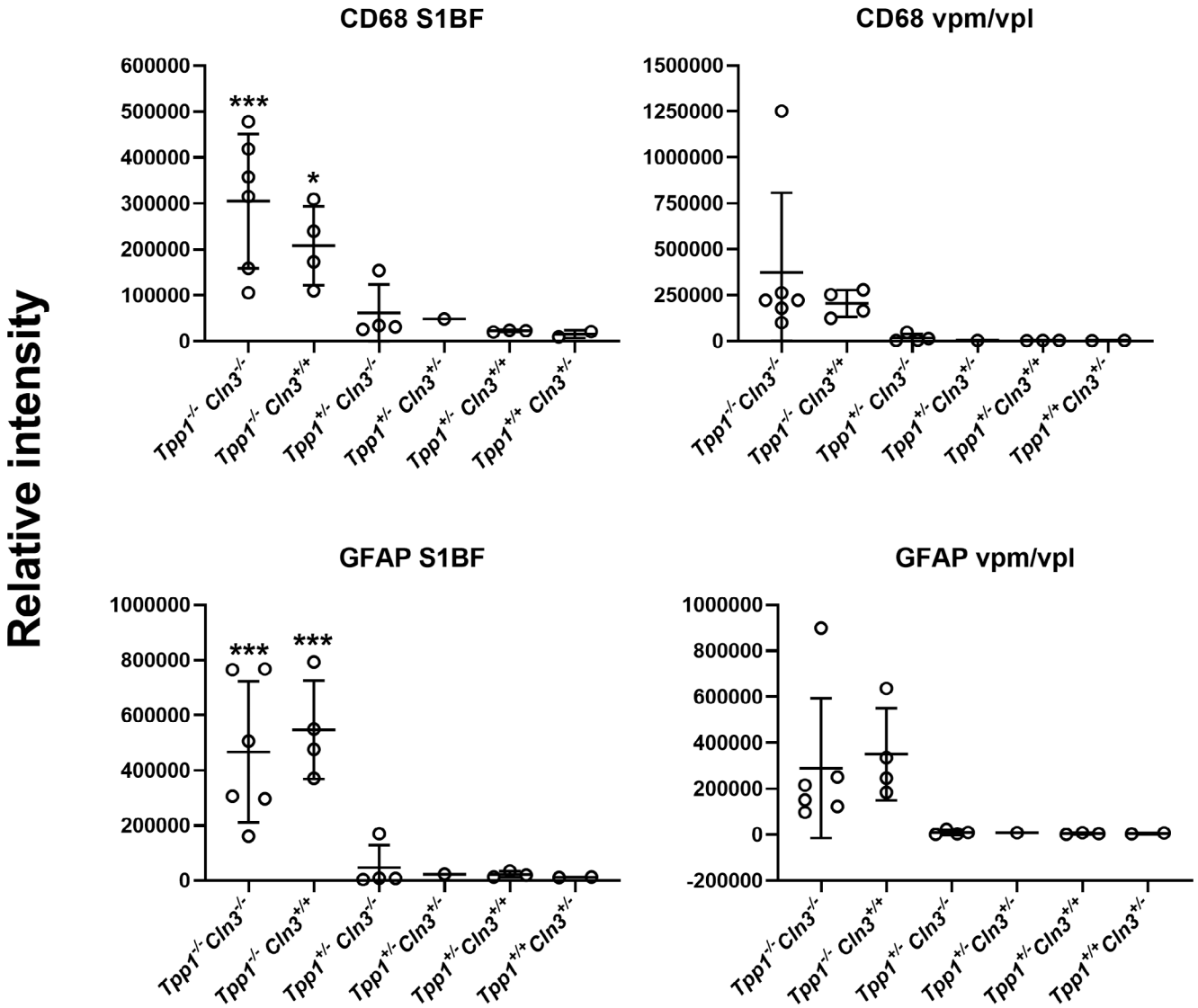

FIGURE 3 Quantitative analysis of glial activation in 120-day old mice. Thresholding image analysis confirms the different levels of glial fibrillary associated protein (GFAP, astrocytes) and CD68 (microglia) in the primary somatosensory cortex (S1BF) and ventral posterior thalamic nuclei (VPM/VPL) of animals of different genotypes. These data confirm the significantly elevated levels of both antigens in $Tpp1^{-/-}Cln3^{+/+}$ and $Tpp1^{-/-}Cln3^{-/-}$ mice compared to animals of other genotypes, which displayed very low levels of immunoreactivity for these markers. *$p < 0.05$ and ***$p < 0.001$ when compared to combined controls $Tpp1^{+/+}$;$Cln3^{+/-}$ and $Tpp1^{+/-}$;$Cln3^{+/+}$ using one-way ANOVA with Dunnett's test for multiple comparisons. Bars indicate mean and standard deviation.

animals (Figure 5A). Relatively few changes were detected in the $Cln3^{-/-}$ mutant animals in $Tpp1^{-/+}$ or $Tpp1^{+/+}$ backgrounds but NPC1 and CTSF were consistently elevated while NEU4 and SMPD1 were decreased (Figure 5B).

3.5 | TPP1 activity in mutant mice

Previous studies have reported elevated TPP1 activities in the brains of *Cln3* knockout mice.[26] Consistent with these earlier studies, we find that TPP1 activity in the *Cln3* mutant is ~2-fold higher than that measured in wild-type animals, while no activity was detectable in $Tpp1^{-/-}$ animals irrespective of *Cln3* genotype (Figure 6). While previous analyses[19] indicated that TPP1 activity in $Tpp^{+/-}$ animals is, as expected, ~50% of wild-type, TPP1 activity in $Tpp^{+/-}Cln3^{-/-}$ animals is ~100% of wild-type. This again indicates that loss of CLN3 results in an ~2-fold increase in TPP1 activity.

4 | DISCUSSION

The overall goal of this study was to determine the phenotype of a double *Tpp1* and *Cln3* mutant mouse model,

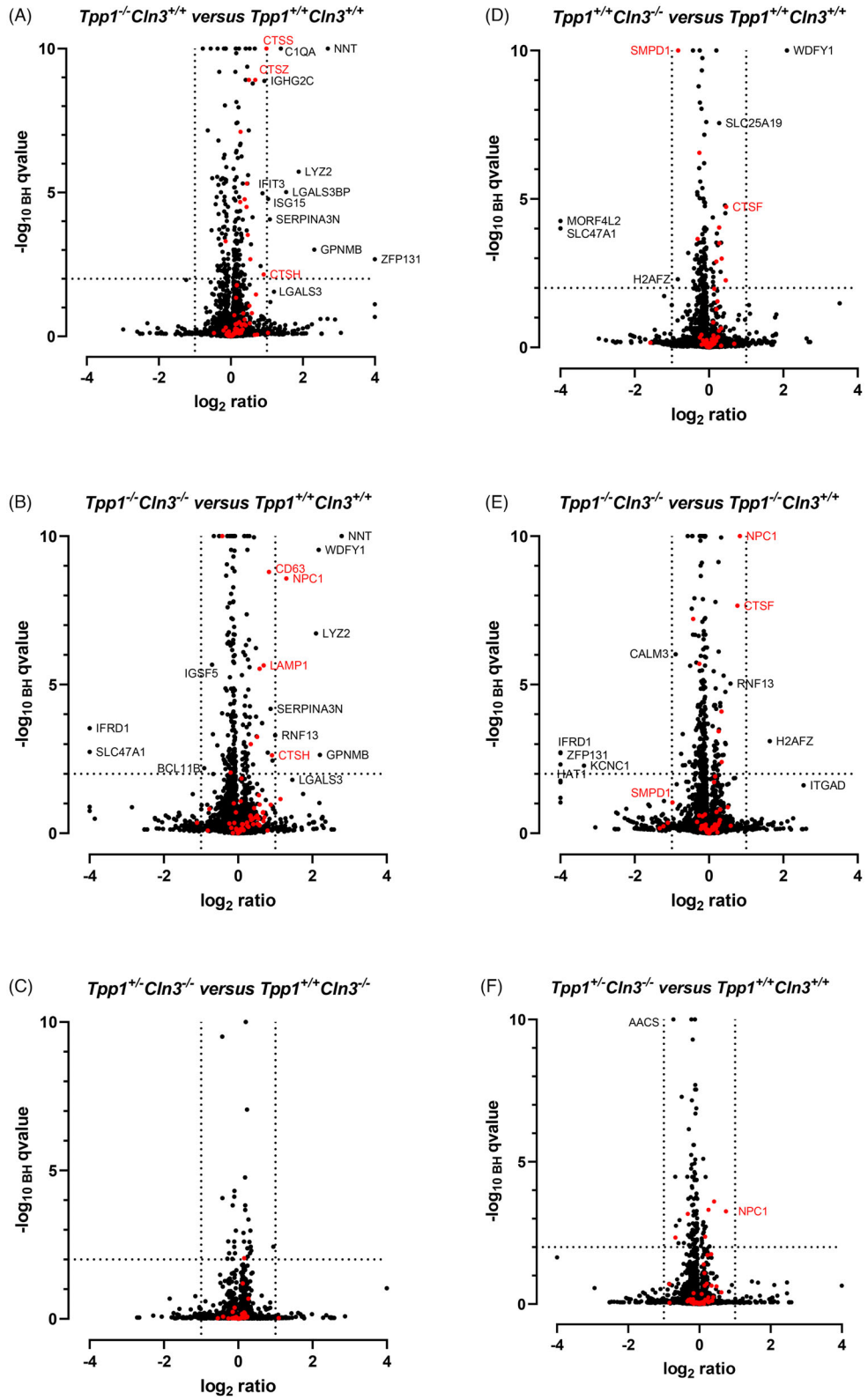

FIGURE 4 Relative protein expression in *Tpp1* and *Cln3* mutant mice determined by SPS-MS3 quantitation of isobaric-labeled peptides. Comparisons are (A) $Tpp1^{-/-}Cln3^{+/+}$ versus $Tpp1^{+/+}Cln3^{+/+}$; (B) $Tpp1^{-/-}Cln3^{-/-}$ versus $Tpp1^{+/+}Cln3^{+/+}$; (C) $Tpp1^{+/-}Cln3^{+/+}$ versus $Tpp1^{+/+}Cln3^{-/-}$; (D) $Tpp1^{+/+}Cln3^{-/-}$ versus $Tpp1^{+/+}Cln3^{+/+}$; (E) $Tpp1^{-/-}Cln3^{-/-}$ versus $Tpp1^{-/-}Cln3^{+/+}$; and (F) $Tpp1^{+/-}Cln3^{-/-}$ versus $Tpp1^{+/+}Cln3^{+/+}$. Q values were calculated based on peptide data for each protein using the False Discovery Rate two-stage step up method of Benjamini, Krieger, and Yekutieli. Dashed lines indicate an FDR of 1% (y axis) and arbitrary fold-change of 2-fold (x axis). Axes are truncated at Q value 1E-10 and ratios of 1/16 to 16. Red and black symbols indicate known lysosomal (based on [17]) and other proteins, respectively. Names of select proteins of interest are shown in red (lysosomal) or black (other).

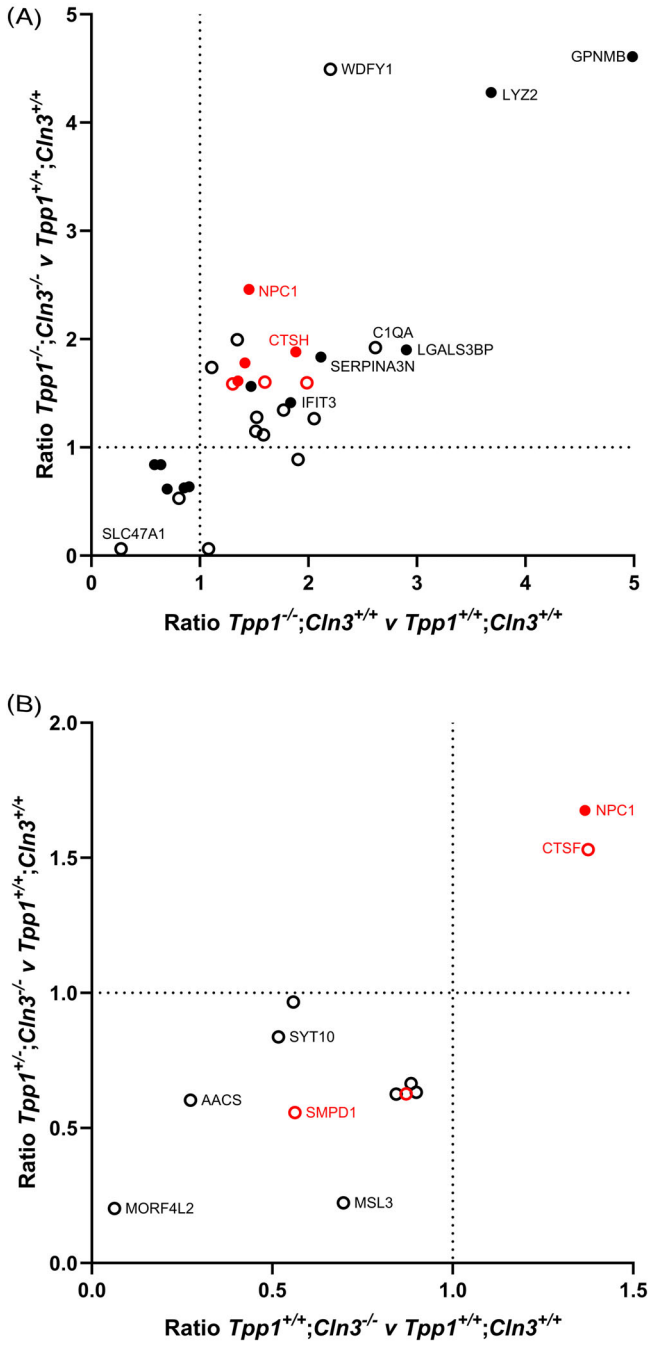

FIGURE 5 Correlation between significant proteomic changes in animals of different genotypes. (A) $Tpp1^{-/-};Cln3^{+/+}$ compared to $Tpp1^{-/-};Cln3^{-/-}$; goodness of fit, R = 0.7901. Note that NNT is censored (see Results). (B) $Tpp^{+/+};Cln3^{-/-}$ compared to $Tpp1^{+/-};Cln3^{-/-}$; goodness of fit, R = 0.5752. Compared to wild-type, proteins shown are significantly altered in at least one model (FDR 1%), have a magnitude of change of ≥1.5 fold in at least one model, and have a consistent direction of change in both models. Names of select proteins of interest are shown in red (lysosomal) or black (other). Filled symbols indicate proteins that are significantly altered in *both* genotypes being compared, open symbols indicate proteins that are significantly altered *in one of the two* genotypes being compared.

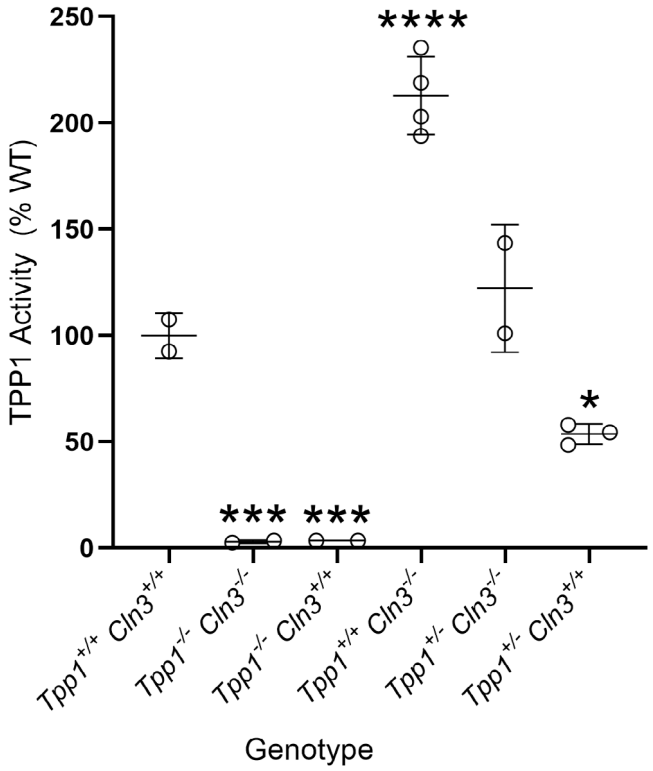

FIGURE 6 TPP1 activity in mutant mice. Activities were measured in brain extracts from 120-day old mice and genotypes were compared to wild-type using one-way ANOVA with Dunnett's test for multiple comparisons when compared to combined controls $Tpp1^{+/+};Cln3^{+/+}$. *$p < 0.05$; ***$p < 0.001$; ****$p < 0.0001$. Bars indicate mean and standard deviation.

which may provide useful information regarding the cellular role of CLN3 and potential functional interactions between TPP1 and CLN3. We find that the phenotype of these double knockout mice was similar or identical to the single *Tpp1* mutant: median survival of both models is within 5 days and they display indistinguishable NCL pathology in the form of astrocytosis and microglial activation.

Glial activation is a consistent pathological feature in NCL diseases, including both LINCL and JNCL.[39,40] Typically, localized glial activation precedes the onset of neuron loss and serves to predict where neurodegeneration subsequently occurs. Indeed, there have been suggestions that glial dysfunction may contribute to neuron loss in multiple NCLs.[40] Quantitative analysis of $Tpp1^{-/-}Cln3^{+/+}$ and $Tpp1^{-/-}Cln3^{-/-}$ mice revealed very similar extents of astrocytosis and microglial activation between mice of these genotypes. In future studies, it will be important to determine whether this similarity extends to the degree of neuron loss in these mice. Such investigations lie beyond the scope of the current study but would further

raise the translational significance of the newly developed mouse model.

Lifespan of the JNCL mouse model (median: 719 days) was somewhat shortened compared to the wild-type (median: 901 days) and this is consistent with previous analysis of a different *Cln3* knockout mouse model (*Cln3*$^{-/-}$, median 742 days, wild-type median 868 days,[36]). Unexpectedly, we found that heterozygosity for *Tpp1* was associated with shortened survival of *Cln3*$^{-/-}$ mice, further decreasing lifespan to a median of 584 days. In addition, survival of a double heterozygote *Tpp1*$^{+/-}$;*Cln3*$^{+/-}$ was also significantly reduced compared to wild-type.

One possible explanation for this observation is that heterozygosity for *Tpp1* exacerbates the *Cln3* phenotype due to substrain effects given that the *Cln3* knockout mouse is in an *Nnt*$^{-/-}$ C57BL/6J background whereas the *Tpp1* knockout is *Nnt*$^{+/+}$ C57BL/6. As a result, the *Tpp1*$^{+/-}$*Cln3*$^{-/-}$ mutant was predicted to be in a mixed *Nnt*$^{+/+}$, *Nnt*$^{+/-}$ and *Nnt*$^{-/-}$ C57BL/6×6J background, and this was confirmed by genotyping *Nnt* in 15 *Tpp1*$^{+/-}$*Cln3*$^{-/-}$ mutants: we found the majority (9/15) to be *Nnt*$^{-/-}$, 5/15 to be *Nnt*$^{+/-}$ and 1/15 to be *Nnt*$^{+/+}$ (data not shown). Thus, most of the *Tpp1*$^{+/-}$*Cln3*$^{-/-}$ animals were in an *Nnt*$^{-/-}$ strain background like the *Cln3*$^{-/-}$ mutant. It is also worth noting that an isogenic *Nnt*$^{-/-}$ C57BL/6J background shortens the lifespan of *Tpp1*$^{-/-}$ animals compared to the same mutation in an *Nnt*$^{+/+}$ C57BL6 background (Figure 1). Thus, if substrain effects were to play a role in survival, we would predict that the introduction of a wild-type *Nnt* allele into the *Tpp1*$^{+/-}$*Cln3*$^{-/-}$ animals would actually *increase rather than shorten* survival of the *Cln3*$^{-/-}$ mouse. Taken together, these observations indicate that substrain effects do not play a role in the shortened survival of the *Tpp1*$^{+/-}$*Cln3*$^{-/-}$ mouse.

Another possibility is that the loss of the CLN3 protein could have adverse downstream effects on TPP1 function or access to its substrates, potentially causing or contributing to JNCL disease. If this is the case, then heterozygosity for *Tpp1* would be predicted to exacerbate disease. The fact that both LINCL and JNCL accumulate SCMAS, a likely primary substrate for TPP1,[41] and the fact that TPP1 activity is elevated in JNCL (Figure 6),[26,42] a possible compensatory response, is consistent with this model. It is also possible that the compensatory increases in TPP1 activity detected in the absence of CLN3 might actually provide a neuroprotective function thus heterozygosity for *Tpp1* would diminish such a protective role, resulting in a shorter lifespan for the *Cln3*$^{-/-}$ mouse. Finally, a recent study[22] indicated that loss of CLN3 results in a lysosomal accumulation of glycerophosphodiesters, and it is possible that increased levels of these lipids directly inhibit TPP1 function. To test this possibility, we conducted assays of increasing amounts of TPP1 in the presence of 100 μM glycerophosphoinositol or 1 mM and 10 mM glycerophosphocholine, two glycerophosphodiesters shown to accumulate in the absence of CLN3. The presence of these lipids had no detectable effect on TPP1 activity in vitro (Figure 7) thus we conclude that they do not directly act as inhibitors at the concentrations tested. However, we cannot exclude the possibility that locally higher concentrations of these accumulated lipids within in the lysosome, or complexes

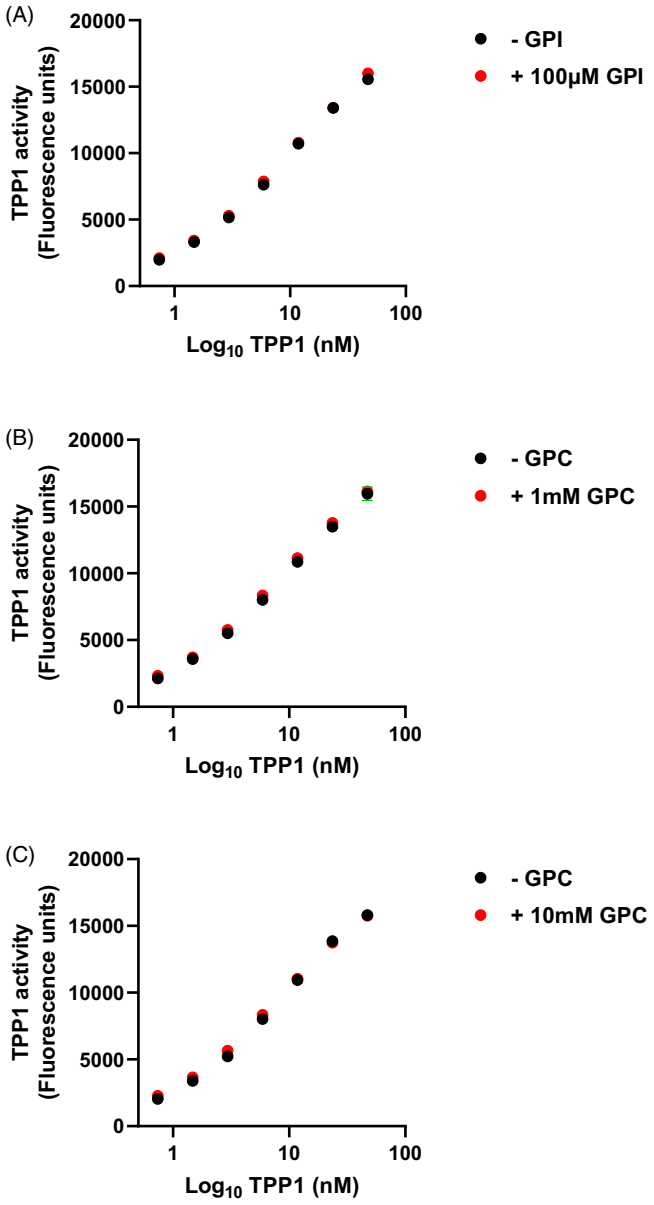

FIGURE 7 TPP1 activity in the presence or absence of glycerophosphodiesters. Activity of indicated amounts of TPP1 was measured by endpoint assay using 200 μM Ala-Ala-Phe-AMC substrate, with or without 1 or 10 mM L-α-glycerophosphorylcholine or 100 μM glycerophosphoinositol.

between these lipids and other lysosomal material, could have an inhibitory effect on TPP1 under physiological conditions.

Regardless of the underlying basis for its shortened lifespan, decreased survival of the *Tpp1*$^{+/-}$*Cln3*$^{-/-}$ mutant may be useful for testing of therapeutic strategies for JNCL. In developing any therapeutic strategy, survival provides a clear and objective endpoint: for example, in evaluating several different strategies for LINCL, survival studies in mouse models have highlighted promising approaches (e.g., gene therapy, intrathecal cerebrospinal fluid [CSF]-mediated ERT, bloodstream mediated ERT)[43–47] while survival studies in the dog model[12] helped pave the way for the approval of enzyme replacement therapy. LINCL animal models have a markedly shortened lifespan thus proof of principle for treatments in terms of survival is readily achievable. In contrast, the survival of *Cln3* mutant mice approaches that of wild-type, complicating survival as an endpoint. As a result, behavioral models have been extensively employed to analyze disease progression and the effects of potential treatment in *Cln3* mutant mice. While numerous studies have characterized locomotor deficits in *Cln3* mouse mutants,[36,48–52] behavioral phenotypes are subtle and are dependent on mouse strain and gender.[49]

Evaluation of potential therapeutics for JNCL in *Cln3*$^{-/-}$;*Tpp1*$^{+/-}$ mouse mutants would provide a relatively robust survival phenotype to measure efficacy. In addition, it is likely that behavioral phenotypes would be exacerbated at a younger age. Effective therapy that addresses the loss of CLN3 (e.g., widespread gene therapy throughout the brain) would be predicted to increase survival of this mouse mutant to resemble that of the *Tpp1* heterozygote, which is indistinguishable from wild-type. A similar approach has been conducted using mutant *Cln3* mice that express human amyloid precursor protein (APP) with familial Alzheimer disease mutations.[53] However, the mutant APP confers a severe survival phenotype even without CLN3 defects, thus positive treatment for CLN3 defects would essentially ameliorate a severe phenotype, not restore wild-type survival.

One goal of this project was to determine whether the double *Tpp1* and *Cln3* knockout could highlight proteomic changes in the brain that could potentially provide a platform for clinically useful biomarkers in either or both LINCL and JNCL. Neurofilament light chain (NEFL in mice) has been proposed as a treatment-responsive biomarker based on studies of plasma from CLN2 patients and a dog model[54] and previously, we found levels of this and other neurofilaments proteins (NEFH and NEFM) to be elevated in mouse CSF.[29] However, we found brain levels of NEFL, NEFH, and NEFM to be unchanged or reduced in the CLN2 and CLN3 mouse models. This is consistent with the finding that brain NEFL is unchanged in mouse models of other neurodegenerative disease exhibiting elevated NEFL plasma and CSF levels.[55] However, this study does reinforce several proteomic changes in LINCL mouse brain that were identified previously including elevated GPNMB, LYZ2, and SERPINA3.[29] Further studies on *Tpp1*$^{-/-}$ mouse models will indicate if any of these proteins are also significantly altered in more accessible biological samples including blood and cerebrospinal fluid. We also found that several lysosomal proteins (CTSF, SMPD1, and NPC1) were significantly altered in the *Cln3*$^{-/-}$ animals and while changes in expression were modest, they may be more evident in older mice (animals were analyzed at ~120 days in this study). These changes may be compensatory responses to the loss of CLN3 and could potentially provide useful information regarding its biological function. In addition, soluble lysosomal proteins SMPD1 and CTSF may also warrant further investigation as potential biomarkers in JNCL.

AUTHOR CONTRIBUTIONS

David E. Sleat: Conceptualization, methodology, formal analysis, investigation, writing—original draft, supervision, guarantor. **Whitney Banach-Petrosky:** Investigation, writing—review and editing. **Katherine E. Larrimore:** Investigation, formal analysis, writing—review and editing. **Yuliya Nemtsova:** Investigation, writing—review and editing. **Jennifer A. Wiseman:** Investigation, writing—review and editing. **Allison Najafi:** Investigation, writing—review and editing. **Dymonn Johnson:** Investigation, writing—review and editing. **Timothy A. Poole:** Investigation, writing—review and editing. **Keigo Takahashi:** Investigation, writing—review and editing. **Jonathan D. Cooper**: Writing—review and editing, supervision. **Peter Lobel:** Conceptualization, methodology, formal analysis, writing—review and editing, supervision.

ACKNOWLEDGMENTS

We thank Dr. Martin Katz (Mason Eye Institute of the University of Missouri School of Medicine) for generously providing survival data for the JNCL mouse model originating from his laboratory.

FUNDING INFORMATION

This project was supported by a grant from the Batten Disease Support and Research Association, Beyond Batten Disease Foundation and Hope 4 Bridget (D.E.S.) and NIH grants R21NS088786 (D.E.S.), R01NS37918 (P.L.), and institutional support from the Department of

Pediatrics, Washington University Medical School, St. Louis (JDC). The authors confirm independence from the sponsors; the content of the article has not been influenced by the sponsors.

CONFLICT OF INTEREST STATEMENT

Peter Lobel and David E. Sleat have received royalty payments as Inventors on Patent 8029781 "Methods of treating a deficiency of functional tripeptidyl peptidase I (CLN2) protein," which is licensed to BioMarin Pharmaceutical Inc. Other authors have declared that no conflicts of interest exist.

DATA AVAILABILITY STATEMENT

Mass spectrometry files (mgf and raw files, GPM search files, and Excel files denoting protein assignments, peptide-spectrum matches, and corresponding reporter ion intensities) are archived in the MassIVE (http://massive.ucsd.edu) and ProteomeXchange (http://www.proteomexchange.org/) repositories in submission MSV000087613. Survival of wild-type C57BL/6 mice was obtained from Jackson Laboratories (https://phenome.jax.org/projects/Yuan2).

ETHICS STATEMENT

Ethics approval was not required for this research study.

ANIMAL RIGHTS

Animals were maintained and used following protocols approved by the Rutgers University and Robert Wood Johnson Medical School Institutional Animal Care and Use Committee protocol I09-0274-4.

ORCID

David E. Sleat https://orcid.org/0000-0002-5159-9928

REFERENCES

1. Mole SE, Williams RE, Goebel HH. *The neuronal Ceroid Lipofuscinoses (Batten disease)*. Oxford University Press; 2011.
2. Sleat DE, Donnelly RJ, Lackland H, et al. Association of mutations in a lysosomal protein with classical late-infantile neuronal ceroid lipofuscinosis. *Science*. 1997;277:1802-1805.
3. Sleat DE, Gin RM, Sohar I, et al. Mutational analysis of the defective protease in classic late-infantile neuronal ceroid lipofuscinosis, a neurodegenerative lysosomal storage disorder. *Am J Hum Genet*. 1999;64:1511-1523.
4. Rawlings ND, Barrett AJ. Tripeptidyl-peptidase I is apparently the CLN2 protein absent in classical late-infantile neuronal ceroid lipofuscinosis. *Biochim Biophys Acta*. 1999;1429:496-500.
5. Sohar I, Lin L, Lobel P. Enzyme-based diagnosis of classical late infantile neuronal ceroid lipofuscinosis: comparison of tripeptidyl peptidase I and pepstatin-insensitive protease assays. *Clin Chem*. 2000;46:1005-1008.
6. Vines DJ, Warburton MJ. Classical late infantile neuronal ceroid lipofuscinosis fibroblasts are deficient in lysosomal tripeptidyl peptidase I. *FEBS Lett*. 1999;443:131-135.
7. Consortium IBD. Isolation of a novel gene underlying batten disease, CLN3. The International Batten Disease Consortium. *Cell*. 1995;82:949-957.
8. Palmer DN, Fearnley IM, Medd SM, et al. Lysosomal storage of the DCCD reactive proteolipid subunit of mitochondrial ATP synthase in human and ovine ceroid lipofuscinoses. *Adv Exp Med Biol*. 1989;266:211-222. discussion 223.
9. de Los RE, Lehwald L, Augustine EF, et al. Intracerebroventricular Cerliponase alfa for neuronal ceroid lipofuscinosis type 2 disease: clinical practice considerations from US clinics. *Pediatr Neurol*. 2020;110:64-70.
10. Schulz A, Ajayi T, Specchio N, et al. Study of intraventricular Cerliponase alfa for CLN2 disease. *N Engl J Med*. 2018;378:1898-1907.
11. Cabrera-Salazar MA, Roskelley EM, Bu J, et al. Timing of therapeutic intervention determines functional and survival outcomes in a mouse model of late infantile batten disease. *Mol Ther*. 2007;15:1782-1788.
12. Katz ML, Tecedor L, Chen Y, et al. AAV gene transfer delays disease onset in a TPP1-deficient canine model of the late infantile form of batten disease. *Sci Transl Med*. 2015;7:313ra180.
13. Passini MA, Dodge JC, Bu J, et al. Intracranial delivery of CLN2 reduces brain pathology in a mouse model of classical late infantile neuronal ceroid lipofuscinosis. *J Neurosci*. 2006;26:1334-1342.
14. Sondhi D, Hackett NR, Peterson DA, et al. Enhanced survival of the LINCL mouse following CLN2 gene transfer using the rh.10 rhesus macaque-derived adeno-associated virus vector. *Mol Ther*. 2007;15:481-491.
15. Worgall S, Sondhi D, Hackett NR, et al. Treatment of late infantile neuronal ceroid lipofuscinosis by CNS administration of a serotype 2 adeno-associated virus expressing CLN2 cDNA. *Hum Gene Ther*. 2008;19:463-474.
16. Crystal RG, Sondhi D, Hackett NR, et al. Clinical protocol. Administration of a replication-deficient adeno-associated virus gene transfer vector expressing the human CLN2 cDNA to the brain of children with late infantile neuronal ceroid lipofuscinosis. *Hum Gene Ther*. 2004;15:1131-1154.
17. Hackett NR, Redmond DE, Sondhi D, et al. Safety of direct administration of AAV2(CU)hCLN2, a candidate treatment for the central nervous system manifestations of late infantile neuronal ceroid lipofuscinosis, to the brain of rats and nonhuman primates. *Hum Gene Ther*. 2005;16:1484-1503.
18. Awano T, Katz ML, O'Brien DP, et al. A frame shift mutation in canine TPP1 (the ortholog of human CLN2) in a juvenile dachshund with neuronal ceroid lipofuscinosis. *Mol Genet Metab*. 2006;89:254-260.
19. Sleat DE, Wiseman JA, El-Banna M, et al. A mouse model of classical late-infantile neuronal ceroid lipofuscinosis based on targeted disruption of the CLN2 gene results in a loss of tripeptidyl-peptidase I activity and progressive neurodegeneration. *J Neurosci*. 2004;24:9117-9126.
20. Sondhi D, Scott EC, Chen A, et al. Partial correction of the CNS lysosomal storage defect in a mouse model of juvenile neuronal ceroid lipofuscinosis by neonatal CNS administration

of an adeno-associated virus serotype rh.10 vector expressing the human CLN3 gene. *Hum Gene Ther*. 2014;25:223-239.
21. Carcel-Trullols J, Kovacs AD, Pearce DA. Cell biology of the NCL proteins: what they do and don't do. *Biochim Biophys Acta*. 2015;1852:2242-2255.
22. Laqtom NN, Dong W, Medoh UN, et al. CLN3 is required for the clearance of glycerophosphodiesters from lysosomes. *Nature*. 2022;609:1005-1011.
23. Cotman SL, Vrbanac V, Lebel LA, et al. Cln3(Deltaex7/8) knock-in mice with the common JNCL mutation exhibit progressive neurologic disease that begins before birth. *Hum Mol Genet*. 2002;11:2709-2721.
24. Katz ML, Shibuya H, Liu PC, Kaur S, Gao CL, Johnson GS. A mouse gene knockout model for juvenile ceroid-lipofuscinosis (batten disease). *J Neurosci Res*. 1999;57:551-556.
25. Langin L, Johnson TB, Kovacs AD, Pearce DA, Weimer JM. A tailored Cln3Q352X mouse model for testing therapeutic interventions in CLN3 batten disease. *Sci Rep*. 2020;10:10591.
26. Mitchison HM, Bernard DJ, Greene ND, et al. Targeted disruption of the Cln3 gene provides a mouse model for batten disease. The batten mouse model consortium [corrected]. *Neurobiol Dis*. 1999;6:321-334.
27. Mekada K, Abe K, Murakami A, et al. Genetic differences among C57BL/6 substrains. *Exp Anim*. 2009;58:141-149.
28. Greene ND, Bernard DL, Taschner PE, et al. A murine model for juvenile NCL: gene targeting of mouse Cln3. *Mol Genet Metab*. 1999;66:309-313.
29. Sleat DE, Wiseman JA, El-Banna M, et al. Analysis of brain and cerebrospinal fluid from mouse models of the three major forms of neuronal ceroid lipofuscinosis reveals changes in the lysosomal proteome. *Mol Cell Proteomics*. 2019;18:2244-2261.
30. Beavis RC. Using the global proteome machine for protein identification. *Methods Mol Biol*. 2006;328:217-228.
31. Craig R, Cortens JP, Beavis RC. Open source system for analyzing, validating, and storing protein identification data. *J Proteome Res*. 2004;3:1234-1242.
32. Sleat DE, Tannous A, Sohar I, et al. Proteomic analysis of brain and cerebrospinal fluid from the three major forms of neuronal ceroid lipofuscinosis reveals potential biomarkers. *J Proteome Res*. 2017;16:3787-3804.
33. Benjamini Y, Hochberg Y. Controlling the false discovery rate: a practical and powerful approach to multiple testing. *J R Stat Soc Series B Stat Methodology*. 1995;57:289-300.
34. Nelvagal HR, Dearborn JT, Ostergaard JR, Sands MS, Cooper JD. Spinal manifestations of CLN1 disease start during the early postnatal period. *Neuropathol Appl Neurobiol*. 2021;47:251-267.
35. Yuan R, Meng Q, Nautiyal J, et al. Genetic coregulation of age of female sexual maturation and lifespan through circulating IGF1 among inbred mouse strains. *Proc Natl Acad Sci U S A*. 2012;109:8224-8229.
36. Katz ML, Johnson GS, Tullis GE, Lei B. Phenotypic characterization of a mouse model of juvenile neuronal ceroid lipofuscinosis. *Neurobiol Dis*. 2008;29:242-253.
37. Hersrud SL, Kovacs AD, Pearce DA. Antigen presenting cell abnormalities in the Cln3(−/−) mouse model of juvenile neuronal ceroid lipofuscinosis. *Biochim Biophys Acta*. 2016;1862:1324-1336.
38. Chang M, Cooper JD, Sleat DE, et al. Intraventricular enzyme replacement improves disease phenotypes in a mouse model of late infantile neuronal ceroid lipofuscinosis. *Mol Ther*. 2008;16:649-656.
39. Bosch ME, Kielian T. Neuroinflammatory paradigms in lysosomal storage diseases. *Front Neurosci*. 2015;9:417.
40. Cooper JD, Tarczyluk MA, Nelvagal HR. Towards a new understanding of NCL pathogenesis. *Biochim Biophys Acta*. 2015;1852:2256-2261.
41. Ezaki J, Takeda-Ezaki M, Kominami E. Tripeptidyl peptidase I, the late infantile neuronal ceroid lipofuscinosis gene product, initiates the lysosomal degradation of subunit c of ATP synthase. *J Biochem*. 2000;128:509-516.
42. Junaid MA, Pullarkat RK. Increased brain lysosomal pepstatin-insensitive proteinase activity in patients with neurodegenerative diseases. *Neurosci Lett*. 1999;264:157-160.
43. Meng Y, Sohar I, Sleat DE, et al. Effective intravenous therapy for neurodegenerative disease with a therapeutic enzyme and a peptide that mediates delivery to the brain. *Mol Ther*. 2014;22:547-553.
44. Meng Y, Sohar I, Wang L, Sleat DE, Lobel P. Systemic administration of tripeptidyl peptidase I in a mouse model of late infantile neuronal ceroid lipofuscinosis: effect of glycan modification. *PLoS One*. 2012;7:e40509.
45. Meng Y, Wiseman JA, Nemtsova Y, et al. A basic ApoE-based peptide mediator to deliver proteins across the blood-brain barrier: long-term efficacy, toxicity, and mechanism. *Mol Ther*. 2017;25:1531-1543.
46. Wiseman JA, Meng Y, Nemtsova Y, et al. Chronic enzyme replacement to the brain of a late infantile neuronal ceroid lipofuscinosis mouse has differential effects on phenotypes of disease. *Mol Ther Methods Clin Dev*. 2017;4:204-212.
47. Xu S, Wang L, El-Banna M, Sohar I, Sleat DE, Lobel P. Large-volume intrathecal enzyme delivery increases survival of a mouse model of late infantile neuronal ceroid lipofuscinosis. *Mol Ther*. 2011;19:1842-1848.
48. Eliason SL, Stein CS, Mao Q, et al. A knock-in reporter model of batten disease. *J Neurosci*. 2007;27:9826-9834.
49. Kovacs AD, Pearce DA. Finding the most appropriate mouse model of juvenile CLN3 (batten) disease for therapeutic studies: the importance of genetic background and gender. *Dis Model Mech*. 2015;8:351-361.
50. Staropoli JF, Haliw L, Biswas S, et al. Large-scale phenotyping of an accurate genetic mouse model of JNCL identifies novel early pathology outside the central nervous system. *PLoS One*. 2012;7:e38310.
51. Weimer JM, Benedict JW, Getty AL, et al. Cerebellar defects in a mouse model of juvenile neuronal ceroid lipofuscinosis. *Brain Res*. 2009;1266:93-107.
52. Wendt KD, Lei B, Schachtman TR, Tullis GE, Ibe ME, Katz ML. Behavioral assessment in mouse models of neuronal ceroid lipofuscinosis using a light-cued T-maze. *Behav Brain Res*. 2005;161:175-182.
53. Centa JL, Jodelka FM, Hinrich AJ, et al. Therapeutic efficacy of antisense oligonucleotides in mouse models of CLN3 batten disease. *Nat Med*. 2020;26:1444-1451.
54. Ru Y, Corado C, Soon RK Jr, et al. Neurofilament light is a treatment-responsive biomarker in CLN2 disease. *Ann Clin Transl Neurol*. 2019;6:2437-2447.

55. Bacioglu M, Maia LF, Preische O, et al. Neurofilament light chain in blood and CSF as marker of disease progression in mouse models and in neurodegenerative diseases. *Neuron*. 2016;91:494-496.

SUPPORTING INFORMATION

Additional supporting information can be found online in the Supporting Information section at the end of this article.

How to cite this article: Sleat DE, Banach-Petrosky W, Larrimore KE, et al. A mouse mutant deficient in both neuronal ceroid lipofuscinosis-associated proteins CLN3 and TPP1. *J Inherit Metab Dis*. 2023;46(4):720-734. doi:10.1002/jimd.12619